RESOURCE

nature neuroscience

Comprehensive transcriptome analysis of neocortical layers in humans, chimpanzees and macaques

Zhisong He[1,10], Dingding Han[1,2,10], Olga Efimova[3], Patricia Guijarro[1], Qianhui Yu[1,4], Anna Oleksiak[1], Shasha Jiang[1], Konstantin Anokhin[5], Boris Velichkovsky[6], Stefan Grünewald[1] & Philipp Khaitovich[3,6–9]

While human cognitive abilities are clearly unique, underlying changes in brain organization and function remain unresolved. Here we characterized the transcriptome of the cortical layers and adjacent white matter in the prefrontal cortexes of humans, chimpanzees and rhesus macaques using unsupervised sectioning followed by RNA sequencing. More than 20% of detected genes were expressed predominantly in one layer, yielding 2,320 human layer markers. While the bulk of the layer markers were conserved among species, 376 switched their expression to another layer in humans. By contrast, only 133 of such changes were detected in the chimpanzee brain, suggesting acceleration of cortical reorganization on the human evolutionary lineage. Immunohistochemistry experiments further showed that human-specific expression changes were not limited to neurons but affected a broad spectrum of cortical cell types. Thus, despite apparent histological conservation, human neocortical organization has undergone substantial changes affecting more than 5% of its transcriptome.

Humans differ from other primates in a number of aspects, most strikingly with respect to their cognitive abilities. The human brain is a highly heterogeneous organ comprising many anatomically and functionally distinct structures. These include the neocortex, a 2–5-mm thick structure covering brain hemispheres. Given that it is the most recently evolved part of the brain, present only in mammals[1], the neocortex might plausibly harbor those changes responsible for uniquely human cognition. Specifically, cognitive functions unique to humans or particularly pronounced in humans have been mapped to specific neocortical areas, including specific areas of prefrontal cortex (PFC), using functional imaging experiments or cases of localized brain damage[2,3].

In search of mechanisms underlying human cognitive abilities, a number of studies have investigated differences in neocortex composition between humans and nonhuman primates at different levels of molecular organization, including gene expression, identifying a number of human-specific gene expression features[4–6]. These studies, performed on bulk tissue samples representing one or more specific neocortical regions, were insufficient to yield a comprehensive picture of the molecular mechanisms underlying human cognition.

The neocortex itself has a complex laminar architecture, traditionally divided into six layers based on visual examination of its histological organization[1]. Neocortical layers differ from each other in terms of both cell type composition and the direction of neuronal connections[7]. Several studies have assessed gene expression in specific cortical layers. More than 5,000 genes were shown to have differential expression across layers in the mouse neocortex based on cortical layer samples dissected using laser capture microdissection (LCM) and measured using microarrays[8,9] or high-throughput sequencing[8]. Similarly, 4,923 genes showed significant expression differences among cortical layers 2–5 when dissected using LCM from ten cortical regions of the macaque brain and measured using microarrays, with most of the differences shared among regions[10].

In addition to transcriptome-wide studies, expression differences among cortical layers in the mouse[11] and human[12] brains have previously been assessed using *in situ* hybridizations, revealing several hundred mouse and 76 human genes showing visibly differential expression among layers. Only one study so far, based on abundance quantification of 39 proteins in four different brain regions (cingulate, primary motor, somatosensory and primary visual cortices) of eight humans and three chimpanzees, examined recent evolutionary changes in gene expression across cortical layers[13]. That study did not quantitatively estimate the protein abundance differences between species in each layer, however. Thus, at present, we still lack systematic analysis of layer-related expression in the human brain, as well as identification of layer-related expression changes unique to the human brain.

To address this, we adopted an experimental procedure allowing comprehensive profiling of transcripts present in different strata of the cortical samples and applied this to assess gene expression in a specific area of human, chimpanzee and macaque PFC across all histologically defined cortical layers and the underlying white matter.

[1]CAS Key Laboratory of Computational Biology, CAS-MPG Partner Institute for Computational Biology, SIBS, CAS, Shanghai, China. [2]Big Data Decision Institute, Jinan University, Guangzhou, China. [3]Skolkovo Institute of Science and Technology, Skolkovo, Russia. [4]University of Chinese Academy of Sciences, Beijing, China. [5]Department of Neuroscience, National Research Center, Kurchatov Institute, Moscow, Russia. [6]School of Life Science and Technology, ShanghaiTech University, Shanghai, China. [7]Max Planck Institute for Evolutionary Anthropology, Leipzig, Germany. [8]Immanuel Kant Baltic Federal University, Kaliningrad, Russia. [9]Comparative Biology group, PICB, SIBS, CAS, Shanghai, China. [10]These authors contributed equally to this work. Correspondence should be addressed to P.K. (khaitovich@eva.mpg.de).

Received 27 June 2016; accepted 17 March 2017; published online 17 April 2017; doi:10.1038/nn.4548

RESULTS

Tissue dissection and transcriptome data set generation

To analyze the transcriptome architecture of neocortical layers, we adopted a tissue dissection and transcriptome reconstruction procedure previously used to analyze complex samples, such as those from embryos or brain tissue[14,15]. Specifically, we dissected tissue cubes containing all neocortical layers and part of the white matter (WM) from the selected PFC region. Special care was taken to dissect samples containing no convolutions. Each tissue cube was then cut into 10 or 16 laminar sections parallel to the layer architecture, from the surface to the WM (**Fig. 1**). From each section, we isolated and sequenced total poly(A)+ RNA (RNA-seq) on the Illumina platform. Transcriptome profiles of individual laminar sections were then combined to reconstruct total gene expression architecture of a neocortical sample. Within this architecture, laminar sections were assigned to specific neocortical layers and WM based on previously identified marker genes.

The collected data comprised two data sets: dataset 1 (DS1), containing samples from four humans, four chimpanzees and four macaques cut into 16 laminar sections; and dataset 2 (DS2), containing samples from two humans and two macaques, as well as duplicated cubes dissected from one human and one macaque individual, cut into 10 laminar sections.

Gene expression quantification

The resulting RNA-seq data constituted approximately 1.2 billion human, 0.8 billion chimpanzee and 1.1 billion macaque reads (**Supplementary Table 1**). To quantify gene expression in humans, chimpanzees and macaques in an unbiased manner, we mapped all RNA-seq reads to the human–chimpanzee–macaque consensus genome. The consensus genome was constructed based on pairwise genome alignment of the human (hg19), chimpanzee (panTro3) and rhesus macaque (rheMac3) genomes and contained only DNA bases conserved among the three species[16].

After discarding genes with maximum expression below 1 read per kilobase per million of total mapped reads or detected in fewer than half of the samples, 19,171 genes annotated in GENCODE database (v17) containing coordinates of human genic regions were classified as expressed in DS1 and 18,272 GENCODE genes in DS2. Of these, 13,602 and 13,128 genes, respectively, were protein-encoding. Altogether, 15,807 genes, including 12,423 protein-encoding genes, were detected in both data sets (χ^2 test, $P < 0.0001$).

Cortical layer assignment in macaques

To assign laminar sections to the six histologically defined cortical layers, we took advantage of microarray data measured in layers two to six (L2–6) of macaque dorsolateral PFC, dissected using LCM[10].

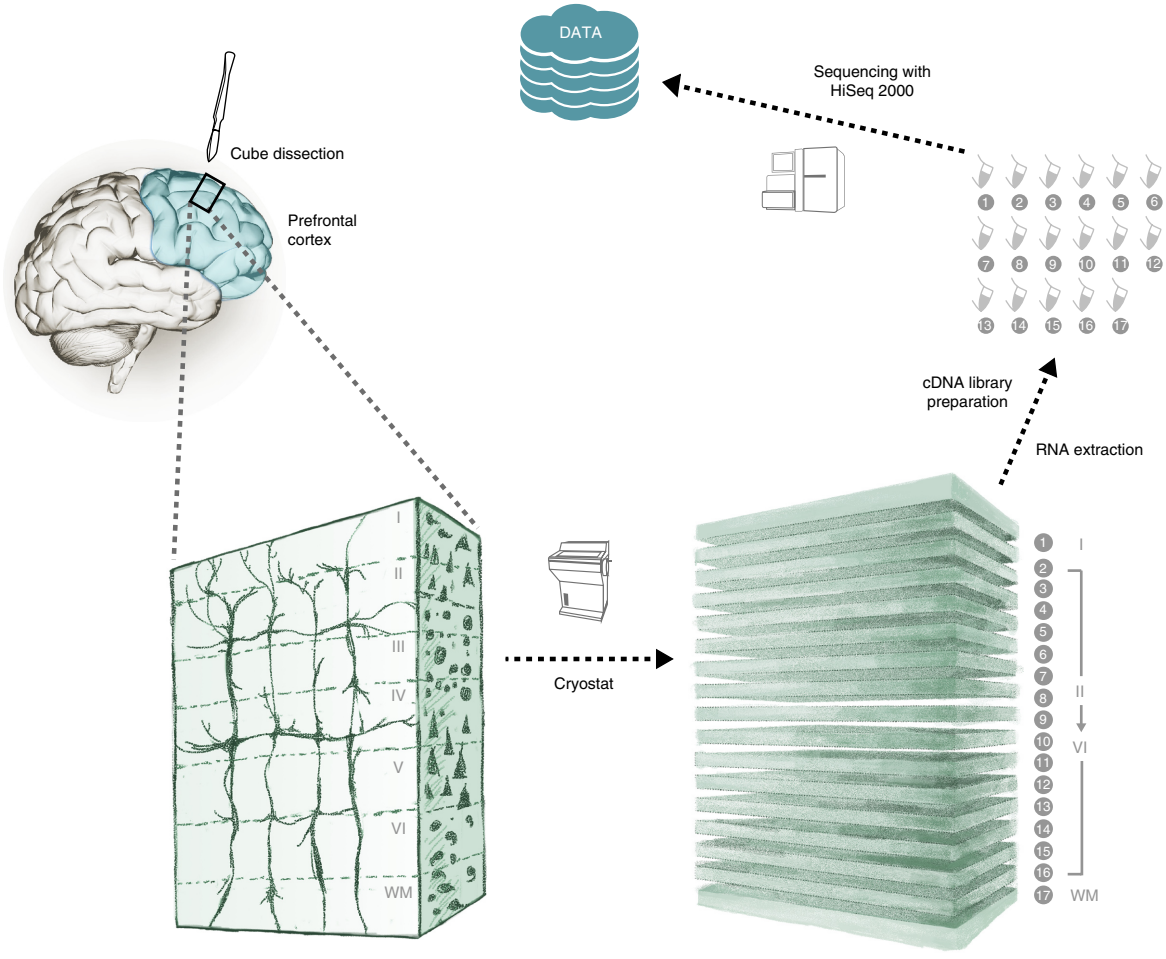

Figure 1 Schematic representation of the methodology for cortical layer transcriptome analysis based on unsupervised sectioning of cortical samples. The dissected PFC samples included a full cross-section of the gray matter (GM) and underlying WM. Each cube was cut transversely using a cryostat. The resulting slices were grouped into 16 (for DS1) or 10 (for DS2) laminar sections from GM and several additional sections crossing the GM–WM boundary. Poly(A)+ RNA from every section was sequenced using the Illumina HiSeq 2000 platform.

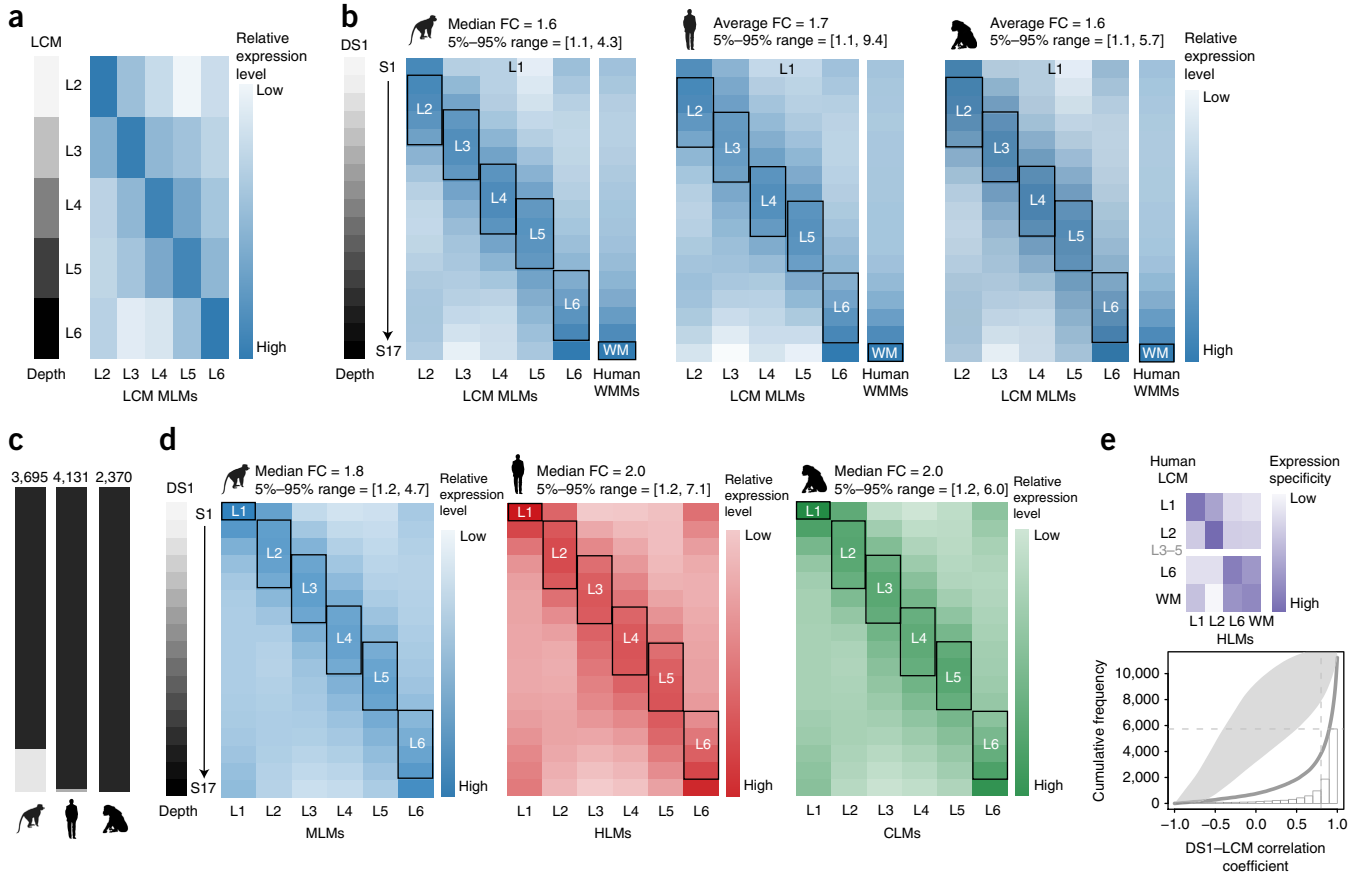

Figure 2 Expression of the layer marker genes. (**a**) Expression of published LCM-based MLMs in the original L2–L6 LCM-dissected samples. (**b**) Expression of L2–L6 LCM MLMs and human WM markers (WMMs) in macaque, human and chimpanzee PFC sections in DS1. (**c**) The proportions of previously uncharacterized layer markers (black) among genes showing layer-related expression in each species in DS1 (numbers on top of each bar). (**d**) Expression of the L1–L6 previously uncharacterized layer markers (previously uncharacterized MLMs, HLMs and CLMs) in the macaque, human and chimpanzee DS1 samples. In **b** and **d**, columns represent cortical layers and WM; rows represent tissue sections obtained using unsupervised sectioning. The gray scale bar shows section labels; the darker shades of gray represent deeper cortical sections. Black boxes and white labels show cortical layer assignments to sections based on LCM MLM and WMM expression. Darker color shades represent higher relative expression of the markers. The median expression fold-change (FC, the median difference between maximum and average expression levels in depicted laminar sections) and its 5–95% range are shown on top. (**e**) HLM expression in human samples dissected using LCM or unsupervised sectioning. Top: heat map shows the expression of L1, L2 and L6 HLMs identified based on DS1, as well as WMMs, in human LCM samples. Darker shades represent higher specificity of HLMs to a given layer. Bottom: the Pearson correlation coefficient (PCC) distribution based on the expression of HLMs identified based on DS1 and LCM samples. The curve shows the cumulative frequency of PCC; the histogram shows the density distribution. Shaded area shows the 95% confidence interval of the cumulative frequency distribution based on 1,000 permutations of the layers; dashed lines show the PCC = 0.8 threshold and the median PCC for the previously uncharacterized layer markers.

Based on reanalysis of these data, we detected expression of 13,347 genes having human orthologs in GENCODE. Of these, 976 showed significant expression differences among layers, and 738 of them were preferentially expressed in a single cortical layer and were classified as macaque cortical layer markers (MLMs; ANOVA, $n = 20$ macaque cortical layer samples, $F_4 > 6.24$, $P < 0.005$, Benjamini–Hochberg (BH)-corrected false detection rate (FDR) < 0.05). In concordance with the laminar organization of the cortex, expression profiles of these MLMs grouped into five expression patterns peaking at the corresponding cortical layers (**Fig. 2a**).

We next investigated the expression of MLMs across the macaque laminar sections generated in our study. To account for differences in cortical layer thickness among samples, section expression profiles were aligned among macaque samples using a modified dynamic time warping algorithm (**Supplementary Table 1**). Of 738 MLMs, 689 were expressed in DS1 and 660 in DS2. The majority showed section-dependent expression in our data: 629 (85.2%) in DS1 (spline-based ANCOVA, $n = 93$ macaque cortical section samples, Holm-corrected $P < 0.05$) and 541 (82.0%) in DS2 (spline-based ANCOVA, $n = 32$ macaque cortical section samples, BH-corrected FDR < 0.05) resulting in a union set of 659 MLMs. Notably, expression of these MLMs in the macaque laminar sections showed distinct expression profiles following the sequence of the cortical layers in both DS1 and DS2, allowing unambiguous assignment of the laminar sections to the histological layers (**Fig. 2b**). The assignment was highly reproducible among samples (**Fig. 3** and **Supplementary Fig. 1**).

While LCM-based MLMs provided information about L2–6 histological layers, our samples were sectioned through the entire depth of the neocortex, from L1 to the underlying WM. To account for this, the first section of each sample was assigned to layer L1, which is of substantial depth in the cortex of humans, chimpanzees and macaques[7]. To define the laminar sections corresponding to the WM, we examined expression of 1,401 genes preferentially expressed in WM identified in a comparison between transcriptomes of human

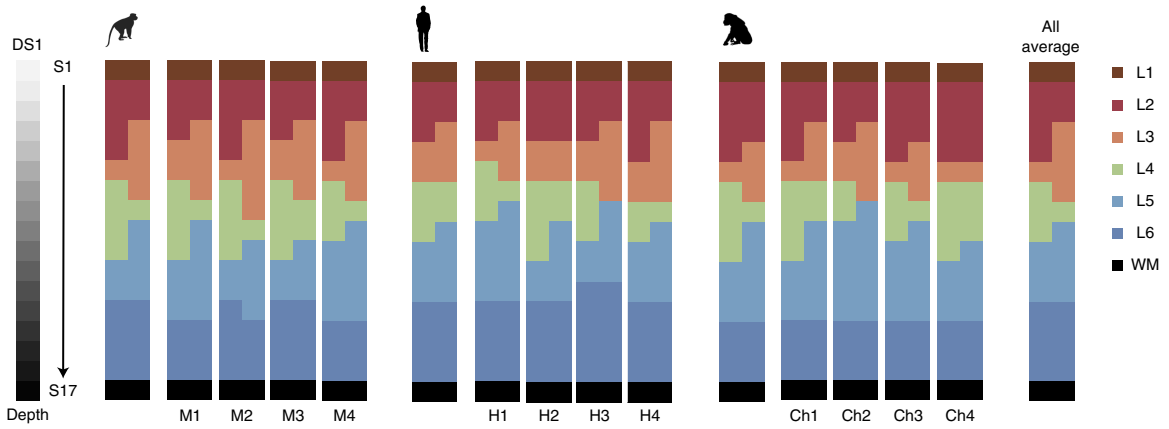

Figure 3 Cortical layer assignments to cortical sections. For each species, marked by silhouette figures, each column represents one PFC sample from DS1. For each species, the leftmost column represents the average cortical sample (S1–17) based on the four individuals of this species (i.e., M1, macaque 1; H1, human 1; C1, chimpanzee 1, etc.). The rows represent tissue sections obtained using unsupervised sectioning; the gray scale bar shows section depth. Darker shades of gray represent deeper cortical sections. The colors represent cortical layer assignment based on relative expression of known MLMs across sections. WM was assigned to sections based on relative expression of the human WMMs. Rows with two colors represent boundary sections with ambiguous layer assignment of samples.

gray and white matters[17]. We detected a clear excess of WM-enriched genes in the deep laminar sections of all three species, allowing us to define the WM boundary.

Identification of previously uncharacterized layer marker in macaques

The 659 MLMs constitute only 6.57% of genes showing section-dependent expression in the macaque cortex in DS1 (spline-based ANCOVA, $n = 93$ macaque cortical section samples, Holm-corrected $P < 0.05$; permutation test, $P < 0.01$, FDR = 0.01%) and 7.90% in DS2 (spline-based ANCOVA, $n = 32$, BH-corrected FDR < 0.05; **Supplementary Table 2**). The assignment of laminar sections to cortical layers allowed us to search for previously uncharacterized MLMs among the remaining section-dependent genes. To do so, we generated six artificial expression patterns specific to one of the defined cortical layers (L1–L6) and defined MLMs as genes correlated to one pattern but not to the other patterns ($r > 0.5$).

Applying this method to all genes expressed in a section-dependent manner in DS1 resulted in 3,187 previously uncharacterized MLMs (**Fig. 2c**). Expression profiles of these MLMs closely resembled those of 629 known MLMs (**Fig. 2d**) and were between the two data sets (median $r = 0.92$; **Supplementary Fig. 2**). Selecting only consistently expressed layer markers (DS1 and DS2 $r > 0.8$, $P < 0.05$) resulted in 2,164 previously uncharacterized MLMs (**Supplementary Table 2**).

Cortical layer assignment in humans and chimpanzees

Previously, gene expression in human cortical layers was only studied using *in situ* hybridizations, producing data for 979 genes and resulting in the identification of 86 genes with layer-dependent expression[12]. To our knowledge, no such studies had been conducted in chimpanzees. We proceeded to identify genes with layer-related expression in human and chimpanzee PFC by (i) assigning human and chimpanzee laminar sections to histologically defined layers, using the bulk of MLMs defined above, and (ii) identifying human and chimpanzee cortical layer markers following the procedure used to previously uncharacterized MLMs.

Following the alignment of expression profiles among human or chimpanzee samples using the modified dynamic time warping algorithm, we identified 11,472 genes showing section-dependent expression in human and 9,299 in chimpanzee laminar sections in DS1 (spline-based ANCOVA, $n = 81$ human cortical section samples and $n = 94$ chimpanzee cortical section samples, Holm-corrected $P < 0.05$). Of these, 7,968 were shared among humans and chimpanzees and 5,892 were shared among all three species (permutations, $P < 0.001$; **Supplementary Fig. 3**). The expression profiles of these 5,892 genes, as well as of all 14,105 genes showing expression differences among laminar sections in at least one species, were strongly and positively correlated between any pair of species (**Supplementary Fig. 3**). This showed that, in agreement with previous work conducted in humans and macaques[8], gene expression profiles of cortical layers are broadly conserved among these primate species. This further implied that the bulk of layer-marker genes defined in macaques can be used to assign laminar sections to cortical layers in humans and chimpanzees.

Indeed, plotting expression of 659 known MLMs or all 3,149 MLMs detected in DS1 in human and chimpanzee laminar sections resulted in distinct layer-related expression patterns arranged in orders corresponding to the cortical layer sequence (**Fig. 2b** and **Supplementary Fig. 3**). The resulting layer assignment was reproducible among human and chimpanzee individuals, as well as among duplicated samples taken from the same individual (**Fig. 3** and **Supplementary Fig. 1**).

To test the validity of this assignment, we used genes showing layer-specific expression in the human temporal cortex, defined based on *in situ* hybridizations[12]. The same study showed close similarity of layer-specific expression between the temporal cortex and the secondary visual cortex area, suggesting conservation of layer-specific expression across most of the cortex, including the PFC. Among the 979 genes examined using *in situ* hybridization, 86 were classified as showing layer specificity[12] and detected in DS1. Of these, 76 genes had laminar section-related expression in humans in DS1 and 67 (88%) showed consistent layer specificity in our data, thus supporting the validity of our layer assignment to the human laminar sections (permutations, $P < 0.001$; **Supplementary Fig. 3**). Furthermore, we checked the expression profiles for nine well-characterized human or mouse layer-marker genes, including *RELN*, *CALB1*, *CALB2*, *RORB*, *ETV1* and *TLE4*[18], as well as one WM marker gene, *SLC5A11*[17] (**Supplementary Fig. 4**). All human markers and the majority of the mouse markers showed consistent layer specificity in our data.

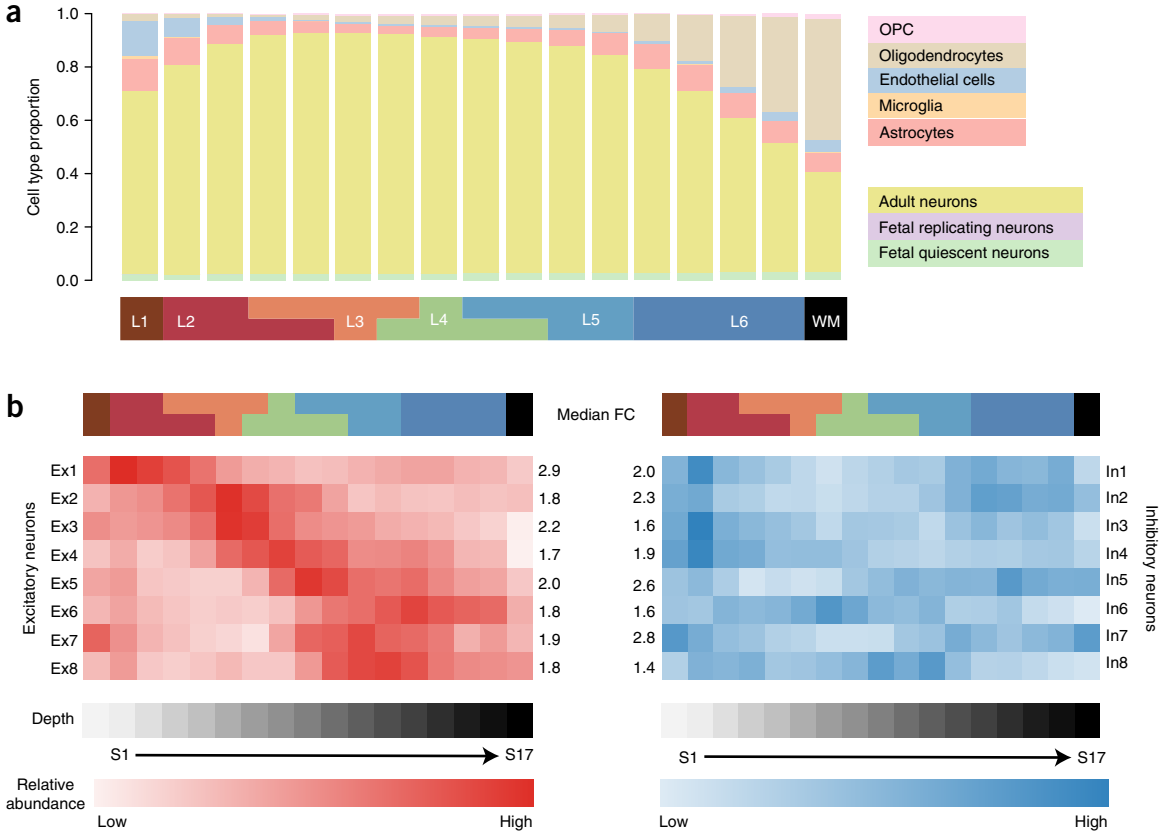

Figure 4 Laminar transcriptome profiles in human PFC represent laminar cell type composition patterns. (**a**) The estimated proportions of mRNAs contributed by each brain cell types by CIBERSORT[19]. Colored bars represent the estimated proportions in each section. (**b**) Average laminar expression patterns of neuron subtype markers[24] in the human PFC. Columns represent tissue sections obtained using unsupervised sectioning; the gray scale bar shows section depth. Darker shades of gray represent deeper cortical sections; darker shades of color represent higher relative expression of the markers: red, excitatory neurons; blue, inhibitory neurons. Ex1–8 and In1–8 indicate subtypes of excitatory and inhibitory neurons, respectively. Rainbow bar represents the cortical layer assignment to cortical sections, with the two rows representing possibly ambiguous layer assignments. Median fold change (FC) shows median difference between maximum and average expression levels in depicted laminar sections.

Identification of previously uncharacterized layer markers in humans and chimpanzees

Identification of previously uncharacterized layer markers in human and chimpanzee PFC (HLMs and CLMs), conducted using the same procedure as for previously uncharacterized MLMs, resulted in 4,131 HLMs and 2,370 CLMs defined based on DS1. The layer specificity scores, calculated as the difference in the correlation of each HLM or CLM with its assigned layer profile compared to that with the adjacent layer profiles, showed substantial specificity of HLMs and CLMs, as well as MLMs, to their respective layers (**Supplementary Fig. 5**). Furthermore, using a twofold cutoff for the difference in expression between the assigned layer and the rest of the layers yielded 1,313 HLMs, 822 CLMs and 844 MLMs, of which 97%, 100% and 77%, respectively, were previously uncharacterized (**Supplementary Table 2**). Using a fivefold cutoff yielded 99 HLMs, 20 CLMs and 93 MLMs, of which 96%, 100% and 91%, respectively, were previously uncharacterized (**Supplementary Table 2**). The layer-specificity of the HLMs was highly consistent between human samples from the two data sets (median $r = 0.88$) yielding 2,350 highly correlated HLMs ($r > 0.8$, $P < 0.05$). Furthermore, the expression of identified HLMs, CLMs and MLMs correlated well, indicating general conservation of layer-related expression among humans, chimpanzees and macaques (**Supplementary Fig. 3**). Hence our study yielded 2,350 HLMs, 2,320 (99%) of them previously uncharacterized, as well as 2,370 CLMs, none of which were previously characterized (**Supplementary Table 2**).

To examine the validity of identified layer markers, we used LCM to cut L1, L2, L6 and WM samples from the PFC of three adult humans and determined their transcriptome composition using RNA-seq. The laminar expression patterns of the 11,472 genes classified as showing laminar section-related expression in humans based on DS1 were highly reproducible in the LCM-based data (**Fig. 2e**). Expression of layer markers determined using unsupervised sectioning was also consistent with the LCM results for all examined layers (**Fig. 2e**).

Cell-type-specificity of laminar expression

To characterize the link between cell type composition differences and gene expression differences among laminar sections, we applied transcriptome deconvolution implemented in CIBERSORT[19] using previously published data[20] as the sources of cell-type-specific expression markers. In agreement with histological organization of the layers, the outermost sections corresponding to L1 and inner sections corresponding to L6 and WM were depleted in neurons and enriched in endothelial cells or oligodendrocytes, respectively (**Fig. 4a**). It has to be noted that the deconvolution procedure provides good estimates of the relative cell type proportions but not of their absolute values. For instance, the proportion of neurons is overestimated by this method[21,22], partially due to higher RNA content in neurons compared to glial cells[23].

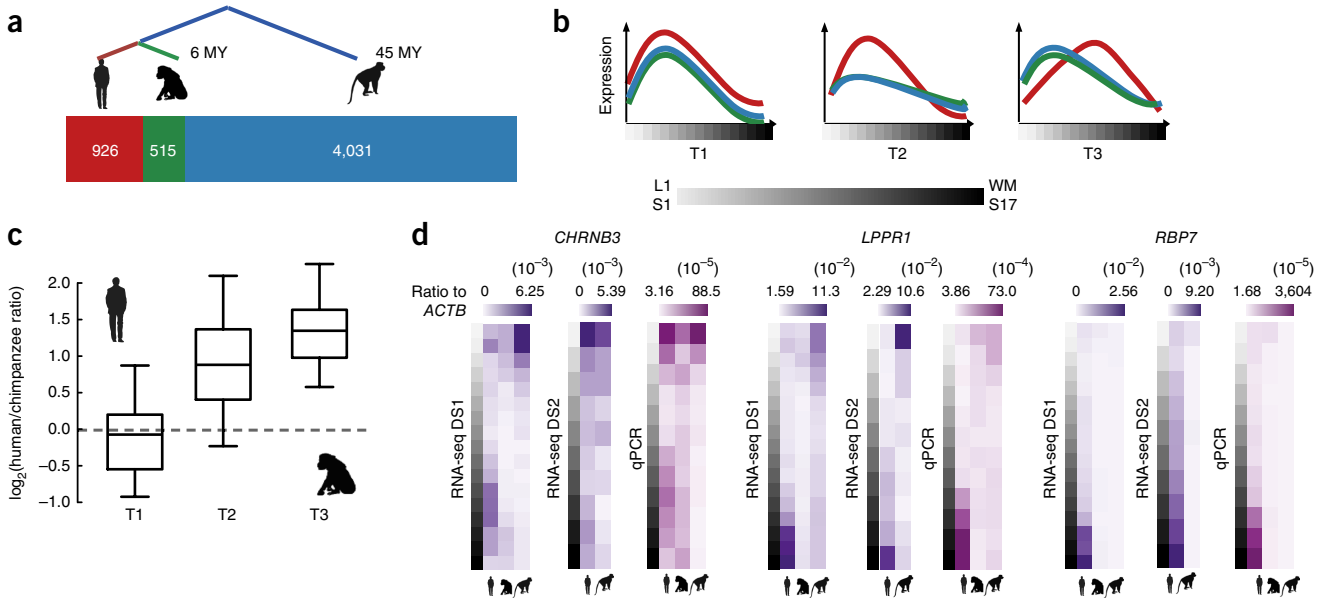

Figure 5 Expression differences among three primate species. (**a**) Numbers of genes showing significant expression changes on the three evolutionary lineages: human (red), chimpanzee (green) and the lineage connecting the common ancestor of humans and chimpanzees with macaques (blue). MY, millions of years since lineage separation. (**b**) Schematic representation of three types of expression changes: T1, constant change across all layers; T2, amplitude changes at specific layers; and T3, changes in layer-specificity. Curves symbolize expression abundances across sections in each of the three species. Horizontal gray scale bars show section depth. (**c**) Ratios of genes assigned to human and chimpanzee evolutionary lineages for each of the three types of expression change. Boxes show $\log_2$-transformed human–chimpanzee ratios based on the numbers of genes assigned to the corresponding lineages and the variation of the ratio estimates calculated using 64× jackknife resampling of cortical samples. Boxes show medians and the upper and lower quartiles; whiskers extend to the maximum and minimum points of the distributions. (**d**) Expressions of genes (*CHRNB3*, *LPPR1* and *RBP7*) showing human-specific expression across cortical layers estimates using RNA-seq data (DS1 and DS2) and qPCR. Darker shades of purple (for RNA-seq data) or pink (for qPCR data) represent higher relative expression across sections. Gray scale bars show section depth; darker shades of gray represent deeper cortical sections.

Notably, even though the middle layers (L2–L5) had similar major cell-type compositions, the neuron subtypes, as previously defined[24], were distributed unevenly across the laminar sections. Notably, excitatory neuronal subtypes formed expression patterns specific to particular layers, while the distribution of inhibitory neuronal subtypes was much less specific (**Fig. 4b**).

Laminar expression differences among species

Of the 14,105 genes showing laminar section-dependent expression in at least one species in DS1, 8,925 (63%) were classified as differentially expressed between humans and chimpanzees (spline-based ANCOVA, $n = 175$ human and chimpanzee cortical section samples, BH-corrected FDR < 0.05). Using macaques as an outgroup, 926 of the 8,925 genes were assigned to the human evolutionary lineage and 515 genes to the chimpanzee evolutionary lineage, while 4,031 genes showed distinct expression in macaques (**Fig. 5a** and **Supplementary Table 2**). The excess of genes with human-specific expression compared to the chimpanzee-specific genes was robust in a samples' Jackknife test ($P = 0.03$), as well as after use of a more stringent definition of expression differences between species (**Supplementary Fig. 6**).

Differential expression detected in ANCOVA included three types of expression change: T1, constant change across all layers; T2, amplitude change at certain layers; and T3, change in layer specificity (**Fig. 5b**). Notably, the proportion of genes assigned to the human and the chimpanzee evolutionary lineages differed starkly among the three types. While T1 genes showed nearly equal distribution of expression changes between the two lineages with slight excess in the chimpanzee-specific genes (human, 125; chimpanzee, 149), T2 genes showed nearly twofold and T3 genes nearly threefold excesses (jackknife resampling, $P < 0.02$) in the human-specific changes (T2: human, 425; chimpanzee, 233; T3: human, 376; chimpanzee, 133; **Fig. 5c**). The excess of T3 human-specific expression changes, as well as absence of such excess for T1 changes, were not caused by differences in RNA quality among samples and were robust to the use of a more stringent definition of expression differences between species (**Supplementary Fig. 6**). Given that T3 genes represent the most radical type of expression change—change in layer-specificity—this result suggests a near threefold acceleration of changes in cortical layer organization in the human lineage.

To test the authenticity of identified changes, we performed quantitative PCR (qPCR) experiments for three genes showing human-specific expression change in cortical slices (12 laminar sections per sample) independently dissected from the brains of three humans, three chimpanzees and three rhesus macaques not used in the RNA-seq experiment. qPCR measurements correlated strongly and positively with RNA-seq-based expression profiles for all three genes (**Fig. 5d**).

Evolutionary changes in gene expression across cortical layers

Assigning changes in the expression specificity of T3 genes to cortical layers revealed a complex picture. First, in all three species, changes in expression layer specificity involving L1 and WM exceeded changes involving the internal layers (L3–L5) by approximately twofold (**Supplementary Fig. 7**). This difference correlated strongly and inversely with the expression of known neuronal marker genes across layers (Pearson correlation, $r = -0.75$, $P = 0.02$; **Supplementary Fig. 7**).

Second, the excess of expression changes in the human lineage compared to the chimpanzee lineage was not caused by a slowdown

of expression evolution in the chimpanzee branch, as the rate of change did not differ between the chimpanzee and macaque lineages (**Supplementary Fig. 7**).

Third, the excess of human-specific expression divergence was not distributed uniformly across layers: in L1 and L5, expression changes were accelerated nearly fourfold, while in L3 and L6, the acceleration was only twofold (**Supplementary Fig. 7**). Unlike the expression divergence rate, human–chimpanzee divergence ratios did not correlate well with neuronal marker expression (Pearson correlation, $r = 0.42$, $P = 0.35$).

Finally, changes in layer specificity occurred with different frequencies between layers. Somewhat unexpectedly, on all three lineages a particularly large number of transitions were observed between L1, the most external cortical layer, and WM (one sided z test, $z = 5.039$, $P < 0.0001$; **Fig. 6a** and **Supplementary Fig. 8**). The human-specific expression transitions between L1 and WM tended to have large-amplitude expression change in DS1: while L1–WM expression transitions accounted for 16% of genes with human-specific T3 changes, they accounted for 45% and 86% for T3 genes with two- and fivefold expression-level laminar differences (**Supplementary Table 2**), respectively (**Supplementary Fig. 8**). Expression of these genes also showed significant positive correlations with LCM-based data ($\rho = 0.34$, $P = 0.008$; **Supplementary Fig. 9**).

In the human lineage, only one type of expression transition stood out among all pairwise comparisons: the transition from L5-specific expression in chimpanzees and macaques to L3-specific expression in humans (L5-to-L3 transition; one-sided Fisher's exact test, $P = 0.08$, odds ratio (OR) = 3.18 for human–chimpanzee comparison; $P = 0.002$, OR = 2.51 for human–macaque comparison; **Fig. 6a** and **Supplementary Fig. 8**). This authenticity of these expression transitions was supported by LCM-based data, using expression in the superficial layers (L2) and the deep layers (L6) as a proxy for outer and inner cortical layers: genes showing human-specific L5-to-L3 transitions were more highly expressed in L2 than in L6 (Fisher's exact test, $P < 0.05$, OR = 6.97). Furthermore, 10 of 14 genes showing human-specific L5-to-L3 transition and detected in the mouse data had significantly stronger specificity to L5 but not to L3 in the mouse cortex using published mouse transcriptome data from cortical layers[8] (**Supplementary Fig. 10**).

Examination of all 1,457 genes with expression specific to L5/6 in the mouse brain[25] showed that the layer specificity of those genes clearly shifts to superficial layers in primates (**Fig. 6b**) and particularly in the great apes (human–mouse comparison: one-sided Fisher's exact test, OR = 1.72, $P < 0.0001$; chimpanzee–mouse comparison: one-sided Fisher's exact test, OR = 1.48, $P < 0.0001$). This concurs with the excess L5-to-L3 transitions in humans and to a lesser extent in chimpanzees, compared to macaques (human–macaque comparison: one-sided Fisher's exact test, OR = 2.9, $P = 0.0008$; chimpanzee–macaque comparison: one-sided Fisher's exact test, OR = 2.0, $P = 0.11$), further suggesting that the deep-layer specificity is the ancestral state.

The 18 genes showing human-specific L5-to-L3 expression transition were enriched in neurons (one-sided Wilcoxon test, $P = 0.047$). Furthermore, co-expression network analysis using WGCNA[26] based on 757 protein-encoding genes showing human-specific laminar expression (**Fig. 7a**) showed that the 16 protein-encoding genes among these 18 genes were overrepresented in two of the six co-expressed modules (M1 and M2; for M1: one-sided Fisher's exact test, OR = 3.98, $P = 0.01$; for M2: one-sided Fisher's exact test, OR = 2.46, $P = 0.03$; **Fig. 7b,c**). Both modules M1 and M2, but not the remaining four modules, showed enrichment trends for markers of pyramidal neurons (uncorrected $P < 0.05$; **Fig. 7b**). This result fits well with our

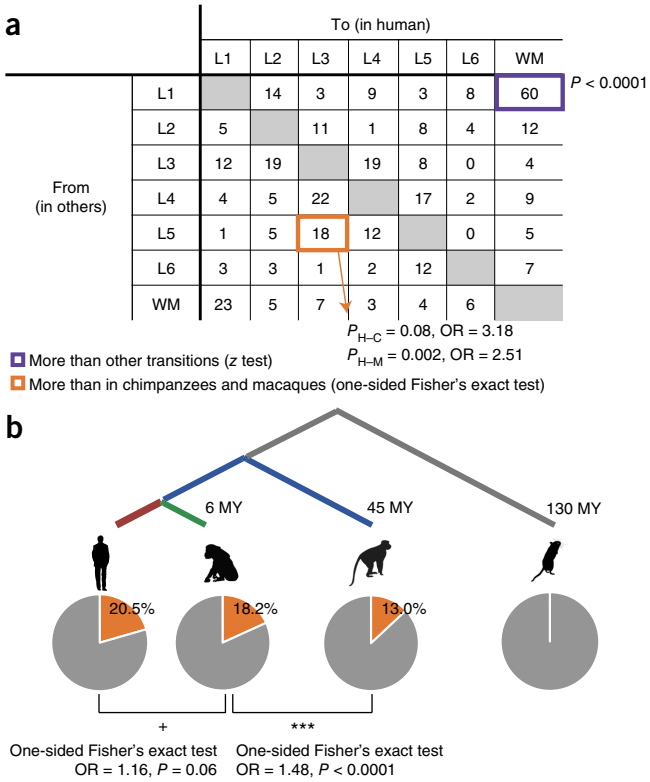

Figure 6 Expression-specificity transitions between cortical layers. (**a**) The numbers of expression-specificity transitions between each pair of cortical layers or WM assigned to the human lineage. (**b**) The proportion of the expression-specificity transitions from the deep cortical layers (L5/6) in mouse PFC to the superficial cortical layers (L2/3) in primate PFC.

hypothesis, which postulated that genes showing L5-to-L3 transition might label and support a unique set of human L3 pyramidal neurons forming human- or primate-specific long-range intracortical projections[12]. The M2 module was also enriched in interneuron markers, suggesting involvement of interneurons in the formation of human-specific cortical architecture. Of the seven total genes previously identified[12] as showing L5-to-L3 expression transition between mouse and human (*COL24A1*, *CRYM*, *BEND5*, *COL6A1*, *PRSS12*, *SCN4B* and *SYT2*), four showed section-dependent expression in our data. Even though none of these four genes passed the statistical definition for the L5-to-L3 transition, all four showed clear shifts from deeper cortical layers in macaques to more superficial layers in chimpanzees and particularly in humans (**Supplementary Fig. 10**).

Notably, genes showing human-specific L1-to-WM transition were significantly overrepresented in module M3 (one-sided Fisher's exact test, OR = 2.45, $P < 0.001$; **Fig. 7b,c**), which is enriched in microglia markers (one-sided Fisher's exact test, OR = 3.06, BH-corrected FDR < 0.001; **Fig. 7b**). This suggested a role for microglia in shaping the organization and function of the human PFC.

Histological analysis of changes in layer specificity

To determine histological localization of proteins linked to genes showing distinct human-specific expression across cortical layers, we randomly selected 11 such genes for immunohistochemistry. Of these 11 genes, nine (six T3 genes and three T2 genes) produced clear immunohistochemistry hybridization signals in the human PFC slices (**Supplementary Fig. 11**). Of these, only three (*CNTNAP4*, *NGB* and *SHC2*) localized in neurons, in agreement with previous results

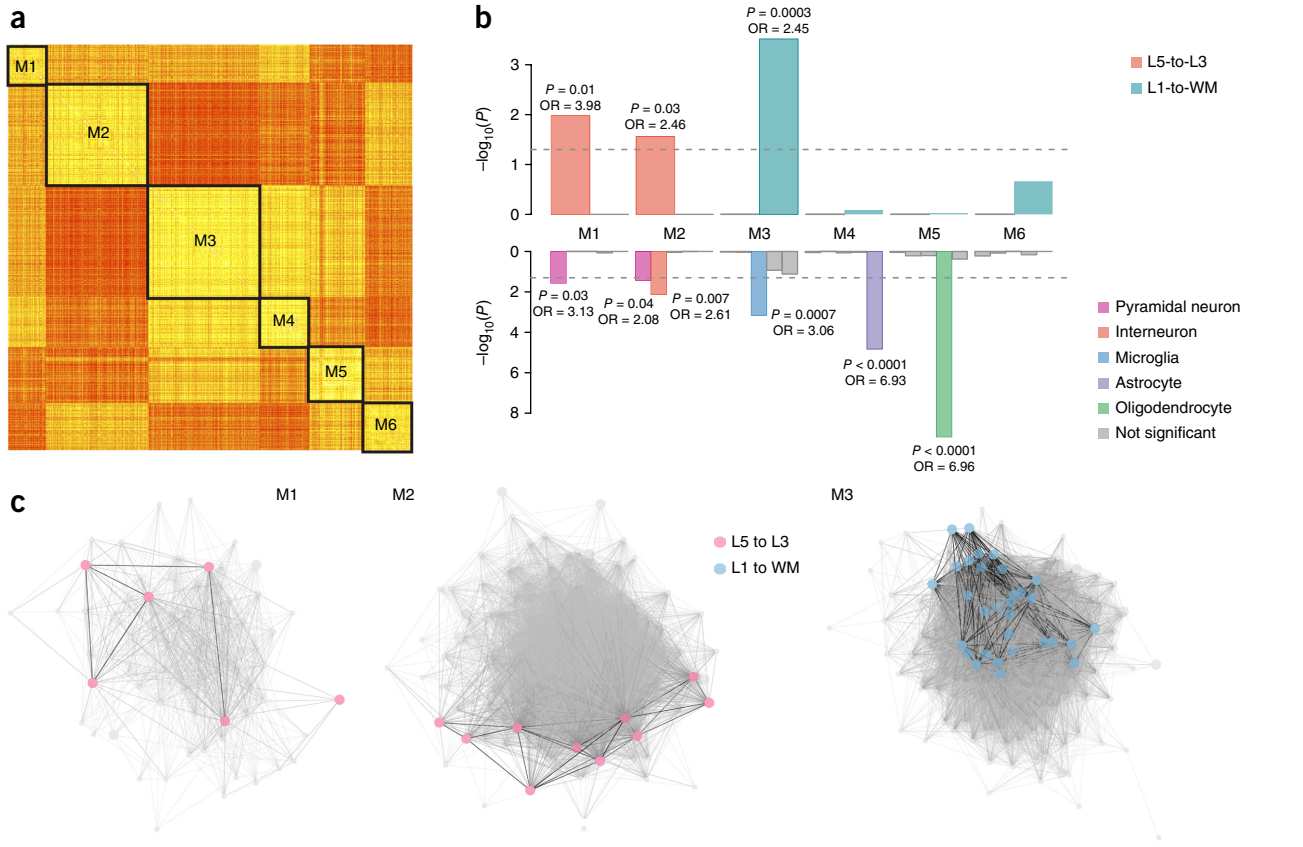

Figure 7 Six modules based on correlated expression across sections of the 757 protein-encoding genes with human-specific laminar expression. (**a**) Pairwise Pearson's correlation coefficients of the genes grouped by the six modules (M). (**b**) Enrichment of cell-type marker genes and genes showing human-specific L5-to-L3 and L1-to-WM transition in the six modules. Bar height shows the negative $\log_{10}$-transformed enrichment test *P* value. Dashed lines represent $P = 0.05$. (**c**) Network diagrams of modules M1 and M2, enriched in genes showing human-specific L5-to-L3 transition (pink) and module M3, enriched in genes showing human-specific L1-to-WM transition (blue). None of the colored nodes are identified as hubs in M1, M2 or M3 modules. Nodes represent genes; edges connect co-expressed pairs with Pearson correlation coefficient > 0.5 ($P < 0.0001$).

based on the transcriptome and proteome measurements[27,28]. The rest were associated with astrocytes (*AQP1*, *CHRNB3* and *NME5*), blood vessel epithelia (*TMEM100* and *SPEF1*) and unidentified varicose protrusions (*CLCN6*; **Fig. 8** and **Supplementary Fig. 11**). The trend of preferential association with astrocytes rather than neurons was further revealed by a general analysis of the cell-type-specificity of T3 genes assigned to the human lineage (one-sided Wilcoxon test, $n_1 = 260$ genes, $n_2 = 10{,}151$ genes, $P = 0.0203$, **Supplementary Fig. 11**) but not to the chimpanzee (one-sided Wilcoxon test, $n_1 = 87$ genes, $n_2 = 10{,}151$ genes, $P = 0.5085$) or macaque (one-sided Wilcoxon test, $n_1 = 1{,}331$ genes, $n_2 = 10{,}151$ genes, $P = 0.9848$) lineages. This suggests that accelerated evolution in the organization of cortical layers in human PFC was not restricted to neurons but affected a large scope of cell types, particularly astrocytes.

DISCUSSION

In this study, we improved histological resolution of cortical transcriptome analysis by assessing changes in gene expression in each of the six histologically defined cortical layers and the underlying WM of humans, chimpanzees and rhesus macaques.

Prior studies focusing on histological examination of cortical organization in humans and other primates did not reveal uniquely human features[29,30]. By contrast, we showed that such features exist at the level of gene expression. Specifically, after the separation of the human and chimpanzee evolutionary lineages, we found that 926 genes changed their expression across cortical layers in a human-specific manner compared to 515 genes that showed chimpanzee-specific changes.

Notably, the type of expression changes particularly pronounced in the human lineage suggested substantial neocortical reorganization. Specifically, gene expression transitions from one layer to another, potentially signifying organizational rearrangements, occurred more than three times as often in the human lineage as in the chimpanzee lineage. Changes enhancing transcriptional specificity to a particular cortical layer were more pronounced in human lineage as well. By contrast, expression-level changes equally present in all layers and reflecting general changes in transcript abundance between species did not show any evolutionary rate imbalances between the two lineages.

Among all possible expression specificity transitions between the layers, the transition from L5 to L3 stood out as the most accelerated in the human evolutionary lineage. Yet even though this transition was unusually frequent in the human lineage, it did not initiate there but instead could be traced all the way back to the separation of primate and mouse lineages. Thus, this case might represent the acceleration of a continuous evolutionary process, potentially reflecting an adaptation to the formation of longer intracortical connections in a larger brain, as proposed[12] based on human–mouse comparisons. This notion was further supported by our observation that genes showing the human-specific L5-to-L3 transition clustered in distinct, co-expressed modules enriched in neuronal markers and specifically

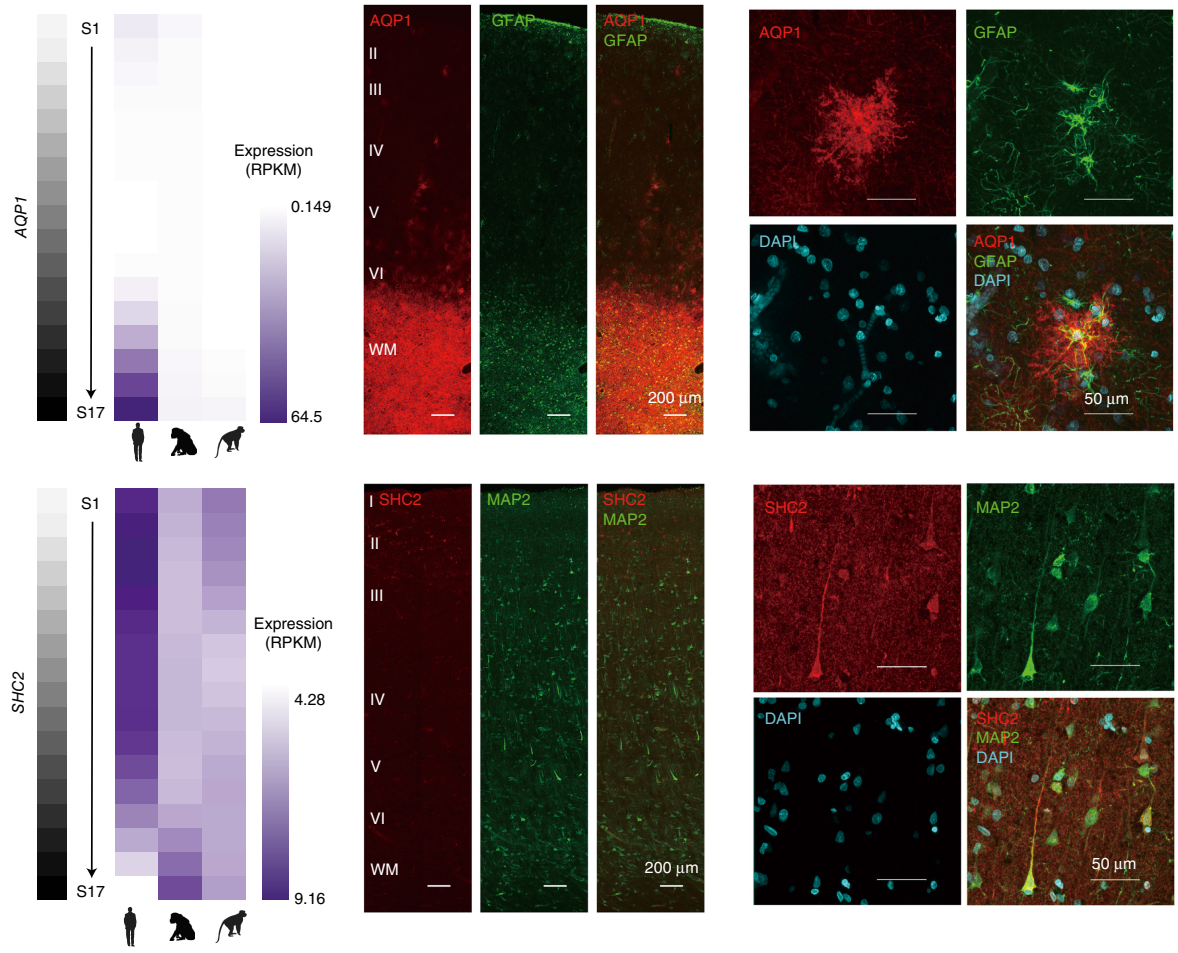

Figure 8 Cell-type specificity of nine selected genes showing human-specific expression. Two examples of immunohistochemistry images from human brain tissues are displayed, showing signals for two of the nine selected genes, *AQP1* and *SHC2*, as well as the astrocyte marker GFAP, neuronal marker MAP2 and general nuclear marker DAPI.

in markers of pyramidal neurons. This is a consistent phenomenon, as previously suggested[12], based on human–mouse comparisons.

Another noteworthy case is the L1-to-WM transition, which accounts for 16% of all human-specific transitions and 19% of the chimpanzee-specific transitions. This was unexpected, considering the distance separating both layers histologically, as well as the different compositions and functions of L1 and WM in the adult PFC[31]. Notably, however, L1 and WM have a common developmental origin: the preplate, a transient structure and the earliest one generated in the developing mammalian neocortex[31,32]. Previous studies have reported different developmental patterns of the preplate and its derivatives, the marginal zone and the subplate, during the evolution of the neocortex[31]. One of the most relevant changes is the relative enlargement of the subplate at the expense of the marginal zone observed in primates, especially in humans, compared to rodents[31,32]. Therefore, the subplate in the human PFC has the largest size and the greatest cellular complexity compared to other species; it persists for a longer period during late gestation compared to primary sensory or motor areas and gives rise to a higher number of interstitial neurons in the adult superficial WM compared to nonassociative cortical areas[33,34]. It is therefore reasonable to speculate that the higher number of expression transitions observed in this study between adult L1 and WM might reflect a recent ontogenetic change, when the asymmetric division of the preplate allowed for an expansion of the subplate, thus providing efficient support for a greater volume of cortical connections. In line with this suggestion, genes showing human-specific L1-to-WM transitions include *PLPPR1* and *EBF4*, which are known to be important in neuron function and neural development[35,36].

Our investigation of cell-type-specificity of genes showing acceleration of expression changes on the human lineage (T3 and T2 genes) revealed broad distribution among cell types. Thus, the neocortical organization features unique to humans are not dominated by neurons but include all cell types, with the enrichment trend for genes expressed in astrocytes and microglia.

In agreement with results obtained in macaques and mice[8,10,11], we found that expression profiles of different layers within the human or chimpanzee neocortex were vastly distinct from one another, as well as from the underlying WM. Comparisons among the cortical layers yielded an extensive list of genes with layer-related expression differences in human, chimpanzee and macaque PFCs, containing a total of 4,470 previously uncharacterized cortical layer markers. The large numbers of genes showing laminar expression patterns, as well as genes classified as layer markers in our study, are due to several methodological differences with those of published works, including: (i) we used spline-based ANCOVA instead of ANOVA as statistical test; (ii) we included L1 and WM laminar sections in the analysis to identify genes with laminar section-related expression, while previous studies mainly focused on L2–L6; (iii) we considered not only

protein-encoding genes but also long noncoding transcripts; 52 of our reported layer markers are long noncoding RNA; and (iv) our sample size is larger than those used in previous studies, resulting in greater statistical power of the tests. Yet our work revealed only a very small fragment of human brain complexity and provides no mechanistic or functional explanations for the expression differences we detected. Nonetheless, it shows that, despite its apparent histological conservativeness, the neocortex harbors many uniquely human gene-expression features. It is not unlikely that at least some of these features reflect changes in cortical organization that make the human brain function differently.

METHODS

Methods, including statements of data availability and any associated accession codes and references, are available in the online version of the paper.

ACKNOWLEDGMENTS

We thank the Maryland Brain Collection Center and the Chinese Brain Bank Center for providing the human samples; the Biomedical Primate Research Centre, the Burgers' Zoo in Arnhem, and R. Martin and W. Scheffran (Zurich University, Anthropology Department, Zurich, Switzerland) for providing the chimpanzee samples; and the Suzhou Drug Safety Evaluation and Research Center and C. Lian, H. Cai and X. Zheng for providing the macaque samples. We thank G.L. Banes for his comments on the manuscript. This study was supported by the Strategic Priority Research Program of the Chinese Academy of Sciences (grant XDB13010200 to P.K.); the National Natural Science Foundation of China (grants 91331203, 31171232, 31501047 and 31420103920 to P.K.); the National One Thousand Foreign Experts Plan (grant WQ20123100078 to P.K.); the Bureau of International Cooperation, Chinese Academy of Sciences (grant GJHZ201313 to P.K.); and the Russian Science Foundation (grant 16-14-00220 to P.K.).

AUTHOR CONTRIBUTIONS

P.K. conceived the project and designed the experiment. Z.H. and Q.Y. designed and executed the bioinformatics analysis. Z.H. designed and executed the bioinformatics analysis. D.H. made sequencing libraries and performed qPCR and LCM experiments. O.E. performed immunohistochemistry experiments. P.G., A.O. and S.J. performed unsupervised sectioning of cortical samples. K.A., B.V. and S.G. contributed to data interpretation. Z.H., D.H., O.E. and P.K. wrote the manuscript.

COMPETING FINANCIAL INTERESTS

The authors declare no competing financial interests.

1. Northcutt, R.G. & Kaas, J.H. The emergence and evolution of mammalian neocortex. *Trends Neurosci.* **18**, 373–379 (1995).
2. Jeon, H.A. & Friederici, A.D. Degree of automaticity and the prefrontal cortex. *Trends Cogn. Sci.* **19**, 244–250 (2015).
3. Jeon, H.A. & Friederici, A.D. Two principles of organization in the prefrontal cortex are cognitive hierarchy and degree of automaticity. *Nat. Commun.* **4**, 2041 (2013).
4. Khaitovich, P., Enard, W., Lachmann, M. & Pääbo, S. Evolution of primate gene expression. *Nat. Rev. Genet.* **7**, 693–702 (2006).
5. Somel, M. *et al.* Transcriptional neoteny in the human brain. *Proc. Natl. Acad. Sci. USA* **106**, 5743–5748 (2009).
6. Liu, X. *et al.* Extension of cortical synaptic development distinguishes humans from chimpanzees and macaques. *Genome Res.* **22**, 611–622 (2012).
7. Defelipe, J. The evolution of the brain, the human nature of cortical circuits, and intellectual creativity. *Front. Neuroanat.* **5**, 29 (2011).
8. Belgard, T.G. *et al.* A transcriptomic atlas of mouse neocortical layers. *Neuron* **71**, 605–616 (2011).
9. Wang, W.Z., Oeschger, F.M., Lee, S. & Molnár, Z. High quality RNA from multiple brain regions simultaneously acquired by laser capture microdissection. *BMC Mol. Biol.* **10**, 69 (2009).
10. Bernard, A. *et al.* Transcriptional architecture of the primate neocortex. *Neuron* **73**, 1083–1099 (2012).
11. Lein, E.S. *et al.* Genome-wide atlas of gene expression in the adult mouse brain. *Nature* **445**, 168–176 (2007).
12. Zeng, H. *et al.* Large-scale cellular-resolution gene profiling in human neocortex reveals species-specific molecular signatures. *Cell* **149**, 483–496 (2012).
13. Bauernfeind, A.L. *et al.* High spatial resolution proteomic comparison of the brain in humans and chimpanzees. *J. Comp. Neurol.* **523**, 2043–2061 (2015).
14. Paul, C.A., Beltz, B. & Berger-Sweeney, J. Sectioning of brain tissues. *Cold Spring Harb. Protoc.* **2008**, ip42 (2008).
15. Peng, G. *et al.* Spatial transcriptome for the molecular annotation of lineage fates and cell identity in mid-gastrula mouse embryo. *Dev. Cell* **36**, 681–697 (2016).
16. He, Z., Bammann, H., Han, D., Xie, G. & Khaitovich, P. Conserved expression of lincRNA during human and macaque prefrontal cortex development and maturation. *RNA* **20**, 1103–1111 (2014).
17. Mills, J.D. *et al.* Unique transcriptome patterns of the white and grey matter corroborate structural and functional heterogeneity in the human frontal lobe. *PLoS One* **8**, e78480 (2013).
18. Hevner, R.F. Layer-specific markers as probes for neuron type identity in human neocortex and malformations of cortical development. *J. Neuropathol. Exp. Neurol.* **66**, 101–109 (2007).
19. Newman, A.M. *et al.* Robust enumeration of cell subsets from tissue expression profiles. *Nat. Methods* **12**, 453–457 (2015).
20. Darmanis, S. *et al.* A survey of human brain transcriptome diversity at the single cell level. *Proc. Natl. Acad. Sci. USA* **112**, 7285–7290 (2015).
21. Pelvig, D.P., Pakkenberg, H., Stark, A.K. & Pakkenberg, B. Neocortical glial cell numbers in human brains. *Neurobiol. Aging* **29**, 1754–1762 (2008).
22. Herculano-Houzel, S. The human brain in numbers: a linearly scaled-up primate brain. *Front. Hum. Neurosci.* **3**, 31 (2009).
23. Filipchenko, R.E., Pevzner, L.Z. & Slonim, A.D. RNA content in the neurons and glia of the hypothalamic nuclei after intermittent cooling. *Neurosci. Behav. Physiol.* **7**, 69–71 (1976).
24. Lake, B.B. *et al.* Neuronal subtypes and diversity revealed by single-nucleus RNA sequencing of the human brain. *Science* **352**, 1586–1590 (2016).
25. Fertuzinhos, S. *et al.* Laminar and temporal expression dynamics of coding and noncoding RNAs in the mouse neocortex. *Cell Rep.* **6**, 938–950 (2014).
26. Zhang, B. & Horvath, S. A general framework for weighted gene co-expression network analysis. *Stat. Appl. Genet. Mol. Biol.* **4**, e17 (2005).
27. Zhang, Y. *et al.* An RNA-sequencing transcriptome and splicing database of glia, neurons, and vascular cells of the cerebral cortex. *J. Neurosci.* **34**, 11929–11947 (2014).
28. Uhlén, M. *et al.* Proteomics. Tissue-based map of the human proteome. *Science* **347**, 1260419 (2015).
29. Alfano, C. & Studer, M. Neocortical arealization: evolution, mechanisms, and open questions. *Dev. Neurobiol.* **73**, 411–447 (2013).
30. Kaas, J.H. The evolution of brains from early mammals to humans. *Wiley Interdiscip. Rev. Cogn. Sci.* **4**, 33–45 (2013).
31. Aboitiz, F., Montiel, J. & García, R.R. Ancestry of the mammalian preplate and its derivatives: evolutionary relicts or embryonic adaptations? *Rev. Neurosci.* **16**, 359–376 (2005).
32. Kostović, I., Judaš, M. & Sedmak, G. Developmental history of the subplate zone, subplate neurons and interstitial white matter neurons: relevance for schizophrenia. *Int. J. Dev. Neurosci.* **29**, 193–205 (2011).
33. Bystron, I., Blakemore, C. & Rakic, P. Development of the human cerebral cortex: Boulder Committee revisited. *Nat. Rev. Neurosci.* **9**, 110–122 (2008).
34. Duque, A., Krsnik, Z., Kostović, I. & Rakic, P. Secondary expansion of the transient subplate zone in the developing cerebrum of human and nonhuman primates. *Proc. Natl. Acad. Sci. USA* **113**, 9892–9897 (2016).
35. Savaskan, N.E., Bräuer, A.U. & Nitsch, R. Molecular cloning and expression regulation of PRG-3, a new member of the plasticity-related gene family. *Eur. J. Neurosci.* **19**, 212–220 (2004).
36. Wang, S.S., Betz, A.G. & Reed, R.R. Cloning of a novel *Olf-1/EBF*-like gene, *O/E-4*, by degenerate oligo-based direct selection. *Mol. Cell. Neurosci.* **20**, 404–414 (2002).

ONLINE METHODS

Samples. The RNA-seq experiments conducted in this study were carried out using RNA isolated from postmortem brain laminar sections that were stored frozen in isopentane/dry ice at −80 °C until the experimental phase. In total, six healthy young adult human (*Homo sapiens*), four healthy young adult chimpanzee (*Pan troglodytes*) and six healthy young adult rhesus macaque (*Macaca mulatta*) brains were used, from which prefrontal cortex (PFC) dissections were obtained. Four samples from each species were selected to generate dataset 1 (DS1) and the remaining samples were used to generate dataset 2 (DS2). Two human samples for DS1 were obtained from the NICHD Brain and Tissue Bank for Developmental Disorders at the University of Maryland, USA. The remaining four samples were obtained from the Chinese Brain Bank Center in Wuhan, China. For each of these individuals, written informed consent to use human tissues for research was obtained either from the donors themselves or from their next of kin. All subjects were classified as normal by forensic pathologists at the brain bank. All subjects suffered sudden deaths with no prolonged agonal state. Use of human autopsy tissue is considered non-human-subject research according to CBBC protocol and is IRB-exempt under NIH guidelines. Chimpanzee samples were obtained from the Anthropological Institute & Museum of the University of Zürich-Irchel, Switzerland, and from the Biomedical Primate Research Centre, Netherlands. Rhesus macaque samples were obtained from the Suzhou Experimental Animal Center, China. All these animals suffered sudden deaths for reasons other than their participation in this study and without any relation to the tissue used. The Biomedical Research Ethics Committee of Shanghai Institutes for Biological Sciences reviewed the use and care of the animals in the research project (approval ID: ER-SIBS-260802P). In humans and chimpanzees, brain tissues were dissected from the anterior superior frontal gyrus (SFG) dorsally to the superior frontal sulcus (SFS) and from the anatomically equivalent region dorsally to the principal sulcus (PS) in macaques (**Supplementary Fig. 12**). Dissected samples mostly corresponded to areas 9 or 10 of Brodmann's map of the cerebral cortex (BA9 or BA10)[37]; in some cases, BA46 was also dissected. The areas selected for dissection have been shown to be histologically as well as functionally similar between monkeys and humans[38,39]. *The Atlas of the Human Brain*[40] and *The Rhesus Monkey Brain*[41] were used to locate samples in human and macaque brains respectively. Since there is no equivalent published resource for the chimpanzee brain, chimpanzee samples were located using *The Atlas of the Human Brain*. Special care was taken to select cubes with WM parallel to the pial surface to avoid gyral curvatures. Final 'cube' samples were kept at −80 °C until being cut in a cryostat. For the human samples used in immunohistochemistry, postmortem brain samples from three male individuals aged 69, 70 and 75 were provided by City Clinical Hospital No. 12 in Moscow, Russia. All three individuals were Caucasians who died of natural causes, having no history of neurological or psychiatric illness. For each of the individuals, written informed consent to use human tissues for research was obtained either from the donors themselves or from their next of kin.

Unsupervised sectioning and RNA-seq. For each individual, one cube or two cubes from a neighboring area were cut out on dry ice. Each cube contained a full cross-section of the gray matter (GM) from the superficial layer 1 (L1) to the deep layer VI (L6) and a portion of WM. Cubes were cut in a cryostat at −25 to −20 °C. The WM part of each cube was embedded in an optimum cutting temperature (OTC) medium, while the gray matter area was in most cases free of the embedding material. If otherwise, the OTC was manually removed from the GM laminar sections during the slicing procedure. The preparations were fixed in an orientation that allowed cutting GM laminar sections parallel to the pial surface. The healthy human, chimpanzee and rhesus macaque cubes were cut into ~50 µm thick slices and then grouped into 16 samples (for DS1) or 10 samples (for DS2), each of which was referred to as one section. This procedure thus resulted in sets of sections with the same absolute section thickness for a given cube and the same relative section thickness between different cubes. The section thickness was 243 µm on average (5.82% of the cube thickness) for the human samples, which is less than the thickness of any cortical layer reported for the human PFC (6.13% for L2 as the minimum[42]; **Supplementary Fig. 12**). The relative thickness relevant to the gray matter thickness was conserved among the three species[43] (**Supplementary Fig. 12**).

One or two additional samples were cut with the same thickness to represent deeper GM or WM for DS1. Each group of samples was immediately placed in 1 mL TRIzol Reagent (Invitrogen, USA) mixed with 50 µL glycogen. The tissue in TRIzol was vortexed until homogenized.

RNA was extracted from every section of every described sample and poly(A) enriched. A TruSeq RNA Sample Prep Kit (Illumina, USA) was used to convert the extracted poly(A)+ RNA into sequencing libraries. The pooled libraries were sequenced on an Illumina HiSeq 2000 platform using a 100-bp singled-ended read module.

Laser capture microdissection and RNA isolation. Cubes of frozen human PFC were embedded in OCT, serially cryosectioned at 30 µm onto PEN Membrane Glass Slides (Applied Biosystems, USA) and stored immediately at −80 °C. Slides were later fixed in 75% ethanol, rinsed in distilled water, stained with cresyl violet, rinsed in distilled water and dehydrated again with 75%, 95% and 100% ethanol. Sections were immediately microdissected using an ArcturusXT Microdissection System (Applied Biosystems, USA). L1, L2, L6 and WM were cut from each of the three human biological replicates. RNA isolation was performed using the PicoPure RNA Isolation Kit (Applied Biosystems, USA) and the CapSure Macro Cap protocol. Libraries were prepared with NEBNext Ultra Low RNA Library Prep Kit (New England BioLabs, USA) and sequenced on the Illumina HiSeq 4000 platform with a 150-bp paired-ended read module.

Consensus genome, read mapping and gene expression estimation. The construction of the consensus genome was performed using the procedure described in He *et al.*[16], with some modifications. Specifically, the chained and netted pairwise genome alignment files of the human (hg19) and chimpanzee (panTro4) genomes and the human (hg19) and macaque (rheMac3) genomes, both aligned by BLASTZ, were downloaded from the UCSC genome browser. Based on these alignments, a human–chimpanzee–macaque multiple genome alignment was constructed using the multiz alignment tool. We then used the three-species alignment to construct a human–chimpanzee–macaque consensus genome by replacing all discordant sites including mismatches and insertions/deletions, as well as 6-bp regions flanking each insertion/deletion sites, with 'N'.

STAR[44] was used to map the raw reads of all samples from all three species to the consensus genome, with default parameters allowing at most 9 mismatches. Only the reads that uniquely mapped to the consensus genome were considered. Multiple reads mapping to the same loci were only counted once.

To estimate gene expression, the same human annotation (GENCODE release 17) was used for human, chimpanzee and macaque samples. To estimate the gene-expression level of genes in the annotation in each sample, we counted reads with at least one nucleotide overlapping with at least one exon of each gene using 'htseq-count'. RPKM (reads per kilobases per million reads) was calculated as $n \times 10^9/LN$, where n is the read counted for the gene, L is the exonic length of the gene and N is the total number of reads that were uniquely mapped to any gene, and the result was used to represent the expression level of each gene in each sample. Transcriptome variance was estimated for each species as the total expression (log-transformed RPKM) variance of all detected genes across all samples of the species. Human and chimpanzee samples had similar variance (human, 411.7; chimpanzee, 414.6).

In order to assess RNA quality directly, we calculated the difference in read coverage between the 3′ and 5′ parts of the transcripts annotated in GENCODE release 17, represented as the 5′-to-3′ read coverage ratio, which is a commonly used RNA-seq-based measure of RNA quality[45] (**Supplementary Table 1**).

Identification of layer-significant genes and markers in macaque with LCM data. All data from Bernard *et al.*[10] coming from macaque DLPFC, with their sample information including layer, sex and individual animal, were downloaded from GEO. Three-way ANOVA, considering factors of layer, sex and individual animal, were applied to identify genes that showed significant changes in each factor.

Genes with significant expression differences among layers, which were referred to as layer-significant genes, were further checked for expression-layer specificity. The expression of each layer-significant gene was compared to five artificially constructed expression patterns, each specific to one of the five layers (L2–L6). Genes with expressions correlating positively and significantly with one of the patterns (Pearson correlation test, $P < 0.05$), but not to the other patterns, were classified as layer markers for the corresponding layer. Genes that were successfully grouped into any gene module were then referred to as LCM-based macaque layer markers (MLMs).

doi:10.1038/nn.4548

The cutoff of correlation to the artificial representative patterns was chosen based on same cutoff used in Bernard *et al*[10]. The distributions of correlations between each known MLM and each artificial representative pattern indicated that $r = 0.5$ provided a reasonable tradeoff between sensitivity and specificity (**Supplementary Fig. 2**). The layer specificity score was defined as $s = r_L - (r_{L-1} + r_{L+1})/2$, where r_L is the correlation between the laminar profile of the marker and the assigned layer L, while r_{L-1} and r_{L+1} are the correlations to the adjacent layers.

Identification of WM-like and GM-like laminar sections. The list of 354 genes upregulated in WM compared to GM and referred to as WM markers was obtained from the work of Mills *et al.*[17]. The elevated expression of WM markers in the laminar sections was defined as being greater than the mean + 1.64× the s.d. of the expression level across all laminar sections of the cube; 1.64 corresponds to the 95th percentile of normal distribution. WM-like laminar sections were then defined, for each cube, as the laminar sections with elevated expression for more than half of the WM markers. The remaining laminar sections were defined as GM-like laminar sections. All GM-like laminar sections located deeper than WM-like laminar sections were excluded from the following analyses.

Identification of section-dependent genes. We tested section-dependent expression per gene by using a spline interpolation model with laminar sections and employing an F test (**Supplementary Software**). For each gene, cubic spline interpolation was used, as implemented in R in the 'smooth.spline' function. As a comparison, we also constructed a null model with uniform expression in all laminar sections. The degree of freedom of the spline interpolation model was chosen from 2 to half of the number of laminar sections, i.e., 8 for DS1 and 5 for DS2 in this study, according to the adjusted r^2 criterion. F tests were used to compare the difference between two models and the alternative models. We used 100 permutations of section indices to estimate permutations-based FDR and significance level at a given nominal P-value cutoff.

Laminar section alignment. To identify the homologous laminar sections, we developed a section alignment algorithm (**Supplementary Software**), with expression patterns of marker genes as input. Marker genes for alignment were initialized as shared section-dependent genes in cubes. They were grouped into clusters using hierarchical clustering, to avoid bias to the large group of genes with similar expression patterns as well as to get more stable anchors for alignment. Clusters that were too small were excluded. The size threshold was determined by the probability of one marker cluster with n genes appearing in random clustering of N genes into m clusters:

$$P = \frac{C_{N-m}^{n-1}(m-1)^{N-m-(n-1)}}{m^{N-m}}$$

With dynamic programming, we defined a dynamic section alignment (DSA) matrix for the alignment between cube X and cube Y as:

$$\mathrm{DSA}_{i,j} = a_{i,j} \times \mathrm{cost}_{X_i,Y_j} + \min(\mathrm{DSA}_{i-1,j}, \mathrm{DSA}_{i,j-1}, \mathrm{DSA}_{i-1,j-1})$$

Here, $a_{i,j}$ is a digital value, set at 0 when there was any cluster with its maximum expression level peak located at section i in cube X and section j in cube Y, and set to 1 when there was no such cluster. Additionally, a locality constraint was introduced by setting a window parameter $w = 4$, so that $|i - j| < 5$, i.e., it was only possible to align two laminar sections (X_i and Y_j) if $|i - j| < 5$. The cost when aligning section i in cube X with section j in cube Y in the section alignment was defined as:

$$\mathrm{cost}_{X_i,Y_j} = \sum_c w_c \, | e_{c,X_i} - e_{c,Y_j} |$$

where $e(c,X_i)$ was the central-scaled average expression level of cluster c in section i of cube X. The weight of each cluster (w_c) was determined by the size of cluster, i.e., $W_c = \sqrt{N_c}$, where N_c is the size of cluster c. The alignment of laminar section series from the two cubes was obtained by tracing back the path to obtain $DSA(N_X, N_Y)$ with N_X and N_Y being the total number of GM-like laminar sections of cube X and cube Y.

When more than two cubes were aligned, the cube with the most laminar sections was used as a template. If multiple options were available, the template was determined as the one resulting in the smallest number of gaps (N_{gap}), i.e., two successive laminar sections in one cube aligned to the same section in the other cube.

Two-step section alignment to align cubes from different species. To align cubes from different species, the section alignment procedure as described above was first applied to cubes coming from each species, referred to as 'within-species alignment'. Based on the within-species alignment, shared section-dependent genes of different samples were identified and their average expression pattern in each species was obtained. The second alignment, which was similar to the first alignment and referred to as 'cross-species alignment', was then applied to different species. The two alignments were integrated, such that a section in a cube was aligned to a certain section in the final template if they were aligned to the same section in the species template.

Mapping cortical layers to laminar sections. The expression patterns of L2–L6 LCM-based MLMs were used to determine the correspondence between layers and laminar sections. For each layer marker gene in the aligned macaque cortical section data, we defined laminar sections with elevated expression as the ones in which marker expression was greater than the mean + s.d. of its expression level across laminar sections in macaques. The number of MLMs with elevated expression at each section was counted for each layer, and a layer was assigned to a section if the section was significantly enriched for MLMs of this layer that showed elevated expression in the section (χ^2 test, $P < 0.05$). Laminar sections with multiple layers assigned were seen as boundary laminar sections, representing the mixture of adjacent layers.

Spline-based test for gene-expression heterospatiality in different species. Genes with significant differences in expression profiles across laminar sections between two species were identified by testing whether a species-differential spline model significantly improved model fitness to the data (**Supplementary Software**). A summary statistic F was used to represent fitting results:

$$F = \frac{RSS_0 - RSS_1}{RSS_1}; RSS_0 = \sum_{g,i} \left(e_{gi} - \bar{e}_{s_i}\right)^2; \; RSS_1 = \sum_{g,i} \left(e_{gi} - \bar{e}_{gs_i}\right)^2$$

where e_{gi} is the expression level of the ith sample in species g, s_i was the section of this sample, $\bar{e}_{s_i}$ was the expected expression level obtained using cubic spline interpolation, as implemented in R in the smooth.spline function with data from both species, and $\bar{e}_{gsi}$ was the expected expression level of species g obtained using cubic spline interpolation with data from species g. The degrees of freedom for spline curve fitting were determined by a generalized cross-validation procedure implemented in smooth.spline.

To calculate P values, we performed 1,000 permutations by randomizing species labels of samples. The same degrees of freedom as used above were used. Each permutation outputs a null statistic, $F^0{}_n$. The P value is calculated by the formula below, where # indicates the number of permutations satisfying the cutoff criteria:

$$P = \mathrm{Pr}_{H_0}\left(F_n^0 > F\right) = \frac{\#\{n : F_b^0 > F, b = 1, \ldots, 1000\}}{1000}$$

Cross validation among data sets. For each gene, Pearson's correlation coefficient (PCC) was calculated between data sets across cortical layers. For DS1 and DS2, the gene expression of a gene in each layer was calculated as the median RPKM of all samples from the cortical sections that corresponded to that layer. For LCM-based data, the average RPKM was calculated for each dissected layer for each gene. Permutations of layers were conducted 1,000 times to estimate the significance of the correlation.

To use the LCM-based data to validate the L3 expression specificity of genes with the human-specific L5-to-L3 transition in DS1, the LCM-dissected L2 and L6 layers were used as proxies to compare the expression of those genes in the superficial layers (L2) to the deep layers (L6). Using a threshold of at least a 1.1-fold change in the average RPKM, we counted the number of genes with higher expression levels in LCM-dissected L2 and the number of genes with higher expression levels in LCM-dissected L6. To test the consistency of L3 expression

specificity, Fisher's exact test was applied, using all genes with human-specific laminar expression as a background.

Classification of lineage-specific changed genes. For each lineage-specific changed gene, the expression level difference at each section was calculated as the difference between the average RPKM in the species with the change and the average RPKMs in the other two species. The spline-based ANCOVA described above to identify section-dependent expression was applied to test the section-dependence of these changes. Genes without significant change of difference across laminar sections (Benjamini–Hochberg corrected FDR > 0.05) were defined as type 1 (T1) genes. The expression level of each layer, as well as the layer with the highest expression level, was then estimated for the species with change and the other species for the remaining genes. Genes with the maximum expression level located in different layers between the species and the remaining two species were defined as type 3 (T3) genes, while the remaining ones were type 2 (T2) genes.

To estimate the robustness of human–chimpanzee divergence ratio we used the jackknife resampling procedure. Specifically, we iteratively subsampled three of the four individuals from each species 64 times and determined genes with lineage-specific expressions using the same procedure as for the full sample set. We then calculated the ratio of the human-specific and chimpanzee-specific differences. The *P* values and variations of the human–chimpanzee divergence ratio estimates were therefore based on jackknife resampling.

Identification of influencing layers. The influenced laminar sections of each gene were defined by the following strategies. The average expression profile of the gene was obtained for the species with specific changes, as well as for the other two species together. The expression level difference between the two average expression profiles was estimated for each section (i.e., d_i for section i). Laminar sections with substantial difference ($|d_i| > \text{mean}_i(|d_i|) + 1.28 \times sd_i(|d_i|)$, where sd is the standard deviation and 1.28 is the 90th percentile of normal distribution) were considered substantially influenced laminar sections. Adjacent laminar sections of the substantially influenced laminar sections were also considered substantially influenced if their difference was no smaller than 90% of the largest difference. If no substantially influenced section was identified, we considered laminar sections with very small differences ($(|d_i| > \text{mean}_i(|d_i|) + 1.64 \times sd_i(|d_i|)$, where 1.64 is the 95th percentile of normal distribution) as infinitesimally influenced laminar sections, with other laminar sections as substantially influenced laminar sections. If no infinitesimally influenced section was identified, the section with the largest difference was considered the only substantially influenced section of this gene. Substantially influenced layers were then defined for each T3 gene, and the layers with at least one assigned section were considered influenced laminar sections.

Cell type enrichment analysis. Two different and complementary methods were used for cell-type-enrichment analysis. The first procedure, marker-based enrichment analysis, was done based on marker genes of nine major cell types, comprising different neuron subtypes including S1 pyramidal neurons, CA1 pyramidal neurons and interneurons, as well as non-neuron glia cells including astrocytes, oligodendrocytes, endothelial cells, ependymal cells, mural cells and microglia, which were identified in mouse brains using single-cell RNA-seq[46]. Hypergeometric tests were applied to compare the enrichment of cell-type markers in the gene list while using all the detected genes as the background.

The second procedure, pattern-based enrichment analysis, was performed based on a meta-analysis of mouse brain cell-type-purified RNA-seq data that covered six major cell types, including neurons, astrocytes, oligodendrocytes, endothelial cells, microglia and oligodendrocyte precursor cells (OPCs)[27]. RPKM was calculated for each gene in each sample, and expression levels across samples were correlated with six binary artificial patterns, each of which represents the expression specificity in one of the six cell types. For each cell type, a one-sided Wilcoxon's rank-sum test was applied to compare the correlation of genes in the gene list to the other genes that were detected in both data.

qPCR to validate human-specific expression profile changes. Three additional cubes from each of the three species were sliced into 12 laminar sections in the cryostat as described above. Total RNA was isolated from the laminar sections with TRIzol (Invitrogen, USA) and reverse-transcribed using SuperScript II reverse transcriptase (Invitrogen, USA) according to the manufacturer's instructions. Quantitative PCR was then performed on a LightCycler 480 system with LightCycler 480 SYBR Green I Master (Roche, Switzerland). The relative mRNA expression level was quantified by the ΔΔCt method. β-actin mRNA was used as an internal control. Randomization and blinding was used for total RNA extraction and qPCR performance. The name and sequences of the qPCR primers are listed in **Supplementary Table 3**.

Immunohistochemistry and imaging. After brain extraction, PFC Brodmann area 10 (BA10) region was dissected from the left hemisphere, sliced into 10-mm thick sections and immediately placed in freshly prepared 4% paraformaldehyde solution at 4 °C for 5 d, rinsed several times in 0.1 M phosphate-buffered saline (PBS; pH 7.4) containing 0.01% sodium azide and stored in the latter solution at 4 °C until further use. The postmortem interval, i.e., the time between death and fixation of the brain sample, was no more than 12 h. Fixed brain samples were cut using a Leica VT1200S vibratome in 30-μm thick serial sections and processed for multiple fluorescent immunohistochemistry, as detailed below. All staining steps were performed in 24-well cell culture plates using individual inserts with permeable bottoms.

For immunofluorescence reactions, the free-floating sections were subjected to heat-induced or room-temperature epitope retrieval procedures specific to each antigen (**Supplementary Table 3**), then washed in 0.1 M PBS (pH 7.4) containing 0.5% Triton X-100 (0.5% PBST) three times for 10 min each time at room temperature (22–24 °C). Then sections were permeabilized for 1 h at room temperature in 1% PBST with 5% normal horse serum (NHS) and 5% normal donkey serum (NDS) and washed again. Reactions with a mixture of primary antibodies (1:250–500; see **Supplementary Table 3**), typically for one human-specific antigen and one glial or neuronal marker, were performed in the blocking buffer (5% NHS, 5% NDS in 0.5% PBST) for 48 h at 4 °C. We stained cellular phenotype markers GFAP for mature astrocytic filaments and ependyma and MAP2 for neuronal cytoskeleton[47,48]. Following washing and incubation with biotinylated horse anti-rabbit/anti-goat/anti-mouse IgG (1:250; manufacturer names and catalog numbers for all antibodies are provided in **Supplementary Table 3**), corresponding to human-specific antigen antibodies, in the blocking buffer for 2 h at room temperature, sections were rinsed in 0.5% PBST and blocked in Image-iT FX Signal Enhancer (Molecular Probes, USA) for 30 min at room temperature to eliminate nonspecific binding of fluorescent conjugates. Washed sections were processed with a mixture of donkey anti-rabbit-Alexa Fluor 488/donkey anti-rabbit-Alexa Fluor 568 or donkey anti-mouse-Alexa Fluor 488/donkey anti-mouse-Alexa Fluor 568 (1:1,000), corresponding to glial or neuronal marker antibody host species and, correspondingly, streptavidin-Alexa Fluor 568/streptavidin-Alexa Fluor 488 conjugate (1:500) for detection of human-specific antigens, overnight at 4 °C. To block lipofuscin autofluorescence, sections were incubated in 1% Sudan black B solution in 70% ethanol for 10 min[49], then washed in PBS, attached to the glass slides, mounted with Fluoromount aqueous mounting medium (Sigma-Aldrich, USA) with the addition of blue fluorescent nuclear counterstain DAPI (0.5 μg/mL, Molecular probes, USA), coverslipped and sealed with nail polish. No staining was seen in control sections processed without the primary antibodies. All antibodies used were guaranteed by their supplier for immunohistochemistry or immunofluorescence in humans.

Images were obtained via an Olympus FluoView FV10i confocal laser scanning microscope with UPLSAPO 60×/1.20-W objective and Olympus FluoView FV1000 confocal system with 20×/0.50-W objective. Image analysis was performed in Imaris v7.2.3 (Bitplane, Switzerland). For each antibody, three images were obtained from each section. Three sections were processed per individual. All repeats yielded reproducible results.

Statistics. No statistical methods were used to predetermine sample sizes, but our sample sizes are similar to those reported in previous publications[8,10]. The experimenters had no knowledge of the samples' species identity during total RNA extraction or library preparation. Laminar section samples from one individual were processed together, while samples from different species and individuals were processed in randomized order and were randomly assigned into different lanes during sequencing.

ANOVA was used to identify macaque cortical layer markers in the LCM data[10]. ANCOVA based on spline interpolation was used to identify

doi:10.1038/nn.4548

section-dependent genes. Permutations were used to calculate the empirical *P* values and FDR at a given nominal *P*-value cutoff. ANCOVA based on spline interpolation and permutation was used to identify genes with heterospatiality in species, where *P* values were estimated by permutations. Jackknife resampling was used to estimate the robustness of the human–chimpanzee divergence ratio. One-sided Fisher's exact tests were used to identify expression transitions with significant excess in human lineage. One-sided *z* tests, based on *z*-transformed numbers of genes with each type of human-specific expression transition, were used to identify transition types with large numbers of transitions. One-sided Fisher's exact tests were also used to compare the enrichment of cell-type markers in the gene list while using all the detected genes as the background to estimate cell-type enrichment. Meanwhile, Wilcoxon's rank-sum test was applied to compare the cell-type specificities of genes in the gene list to those of the background.

A **Supplementary Methods Checklist** is available.

Code availability. The source codes for the section alignment procedures and the spline-based ANCOVA are available at http://www.picb.ac.cn/Comparative/data_methods/data_layer_2017.html.

Data availability. Primary sequence data of this study has been deposited in SRA with project code SRP065273 and BioProject accession code PRJNA299472. The processed gene expression data are available at http://www.picb.ac.cn/Comparative/data_methods/data_layer_2017.html.

37. Brodmann, K. *Brodmann's Localisation in the Cerebral Cortex* (Springer, 2006).
38. Petrides, M. Lateral prefrontal cortex: architectonic and functional organization. *Philos. Trans. R. Soc. Lond. Biol. Sci.* **360**, 781–795 (2005).
39. Sallet, J. *et al.* The organization of dorsal frontal cortex in humans and macaques. *J. Neurosci.* **33**, 12255–12274 (2013).
40. Mai, J.K., Majtanik, M. & Paxinos, G. *Atlas of the Human Brain* 4th edn. (Elsevier, 2016).
41. Paxinos, G., Huang, X.-F., Petrides, M. & Toga, A.W. *The Rhesus Monkey Brain in Stereotaxic Coordinates* 2nd edn. (Elsevier, 2009).
42. Rajkowska, G. & Goldman-Rakic, P.S. Cytoarchitectonic definition of prefrontal areas in the normal human cortex: I. Remapping of areas 9 and 46 using quantitative criteria. *Cereb. Cortex* **5**, 307–322 (1995).
43. Semendeferi, K., Armstrong, E., Schleicher, A., Zilles, K. & Van Hoesen, G.W. Prefrontal cortex in humans and apes: a comparative study of area 10. *Am. J. Phys. Anthropol.* **114**, 224–241 (2001).
44. Dobin, A. *et al.* STAR: ultrafast universal RNA-seq aligner. *Bioinformatics* **29**, 15–21 (2013).
45. Wang, L. *et al.* Measure transcript integrity using RNA-seq data. *BMC Bioinformatics* **17**, 58 (2016).
46. Zeisel, A. *et al.* Brain structure. Cell types in the mouse cortex and hippocampus revealed by single-cell RNA-seq. *Science* **347**, 1138–1142 (2015).
47. Korzhevskii, D.E., Otellin, V.A. & Grigor'ev, I.P. Glial fibrillary acidic protein in astrocytes in the human neocortex. *Neurosci. Behav. Physiol.* **35**, 789–792 (2005).
48. Lyck, L., Dalmau, I., Chemnitz, J., Finsen, B. & Schrøder, H.D. Immunohistochemical markers for quantitative studies of neurons and glia in human neocortex. *J. Histochem. Cytochem.* **56**, 201–221 (2008).
49. Schnell, S.A., Staines, W.A. & Wessendorf, M.W. Reduction of lipofuscin-like autofluorescence in fluorescently labeled tissue. *J. Histochem. Cytochem.* **47**, 719–730 (1999).